ECCOMAS Thematic Conference on Multibody Dynamics
June 19-22, 2017, Prague, Czech Republic

Kinematic validation of a human thumb model

Uday D. Phutane[1], Michael Roller[2], Staffan Björkenstam[3], Joachim Linn[2], Sigrid Leyendecker[1]

[1]Chair of Applied Dynamics
University of Erlangen-Nuremberg
Immerwahrstr. 1, 91058 Erlangen, Germany
[uday.phutane, sigrid.leyendecker]@fau.de

[2]Fraunhofer ITWM
Fraunhofer Platz 1,
67663 Kaiserslautern, Germany
[michael.roller, joachim.linn]@itwm.fraunhofer.de

[3]Fraunhofer-Chalmers Centre
Chalmers Science Park
SE-412 88 Göteborg, Sweden
staffan@fcc.chalmers.se

Abstract

The human thumb is a three-link and three-joint multibody system. Two joints resemble a saddle with two degrees of freedom (DoFs) each, while the third joint is a single DoF joint like a revolute. The two DoFs joints have been modeled as universal joints in many biomechanical works, however anatomically they have axes that are non-intersecting and non-orthogonal. These axes enable the thumb to perform complex motions and to produce the necessary thumb tip forces. Our aim is to develop a biomechanical model of the thumb with the anatomically feasible joint setup. To validate the kinematics of the system, we perform two tests. Firstly, we move the thumb by changing the values of all the DoFs through two different ranges of motions, namely the maximum range of motion (RoM) and the grasp RoM. The grasp RoM is smaller than the maximum RoM. Hence, the grasp RoM volume is lesser than the maximum RoM and this volume reduction is a kinematic measure of the thumb, which we compare for five models (with same joint designs but different axes locations and orientations) with data from literature. Further, the rotation around its longitudinal axis of the thumb can be measured for the thumb in different postures. The thumb joints in themselves do not have a rotation DoF around the longitudinal axis. For different postures, we compute this rotation of the thumb, which we compare with data from literature. In both tests, the results obtained from simulation are in close agreement with literature data and consequently the thumb model's kinematics is validated.

Keywords: thumb kinematics, thumb internal rotation, range of motion, point clouds, anatomically variable thumb models.

1. Introduction

The human hand is the end effector for the upper extremity performing the all important function of grasping. Grasping is a unique function exhibited primarily by primates, through the versatility of motion provided by the thumb and its motions such as opposition and circumduction. The thumb is responsible for over 50% of the hand function, see [1]. The opposition and circumduction motions are a combination of the basic movements of the thumb, such as flexion-extension (flex-ext) and adduction-abduction (add-abd). For the three joints in the thumb, the flex-ext motion is displayed by all the joints, while two joints exhibit the second motion of add-abd. These two joints show a third motion of pronation-supination (pro-sup) or internal rotation along their longitudinal axes during the combined motions, which is not an inherent DoF of the thumb joints, rather an outcome, see [2].

To develop a multibody model of the hand which is very well equipped for grasping simulations, there is a need to be as anatomically correct as possible, as the underlying motions are complex. Many biomechanical models presented until now, e.g. in [3, 4, 5] and others, have described the two DoFs joints as universal joints. This mathematical joint, by design, however does not allow for internal rotation, which some researchers, see [15, 26], have incorporated through an additional DoF. Chang in [15] has discussed that a 3 DoFs joint shows an improved prediction for the internal rotation over the 2 DoF kinematic model, while defining the internal rotation axis as the common perpendicular to the carpometacarpal (CMC) joint flex-ext and add-abd axes. It has been subsequently shown by measurements in cadaver experiments described in [6, 7], magnetic resonance imaging (MRI) described in [17, 18] and through a number of experiments, see [10, 16, 22], that the complex thumb motions are achieved through joints which have non-intersecting and non-orthogonal axes. Although there is a consensus among researchers today about the anatomy of the axes, there is no consensus on their location and orientation. For example, for the CMC joint, axes descriptions have been provided by [6, 9, 14, 15]. Though this has been attributed to the natural variation in the human population, it makes having generic numerical values for a thumb model very challenging.

In this work, we investigate the kinematic behavior of such a generic (base) thumb model and four variations. We create a thumb multibody model using data from cadaver measurements and describe two validation methods to assure

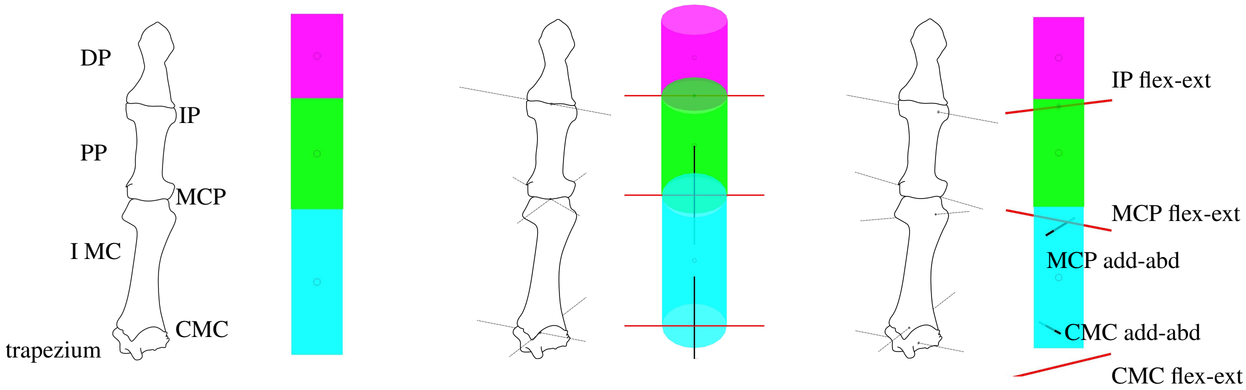

Figure 1: The thumb anatomy with bone and joint nomenclature as introduced in Section 2.1 is shown on the left. The thumb anatomy and associated model with universal joints for the MCP and the CMC, and IP axis perpendicular to the DP is shown in the middle. The thumb anatomy and associated model with anatomically correct joints is shown on the right.

proper thumb kinematics. The first method involves the comparison of work-space point cloud volumes generated by the thumb tip, which are computed using α-shapes. These values are computed for the base thumb model and four other anatomically variable models, obtained from [12]. We compare the volume reduction of the grasp RoM with respect to the maximum RoM for the different thumb models. The second method quantifies the internal rotation in the thumb for different postures and compares them with physical measurement data given in [2], as well as with the anatomically variable models.

The paper begins with the description of the thumb anatomy (Section 2.1), followed by the thumb multibody model (Section 2.2). A detailed description is provided for one of the CMC rotation axes to understand anatomical variance. This variance, when accounted for all rotation axes, leads to the four anatomically different thumb models. After describing the two sets of limits or RoMs (Section 2.3), we describe the two validation techniques (Section 3). The results are presented and discussed (Section 4.1 and Section 4.2). We conclude in Section 5.

2. Thumb anatomy and multibody model

This section describes the anatomy of the thumb and the anatomically corresponding multibody model. We introduce a joint configuration to approximate the CMC and the MCP joints. Following this, we discuss the need for two different limits on the RoM.

2.1. Thumb anatomy

Anatomically, the thumb is composed of three bones, as shown in Figure 1 (left). From the base to the tip of the thumb, they are the first metacarpal (I MC), the proximal phalanx (PP) and the distal phalanx (DP). They are connected in series by three joints with the trapezium bone in the wrist. The CMC, or trapeziometacarpal joint connects the trapezium and the I MC, the metacarpophalangeal (MCP) joint connects the I MC and the PP, while the interphalangeal (IP) joint connects the PP and the DP. The MCP and the CMC are saddle joints and have two rotational DoFs, while the IP has a single rotational DoF. All three joints have the motion of flex-ext, while the CMC and the MCP have the second motion of add-abd. The motion of flex-ext is motion of the thumb out of the plane of the palm and downwards (flexion) or upwards (extension). The motion of add-abd is motion of the thumb in the plane of the palm and towards the palm (adduction) or away from the palm (abduction).

Although the motion between the bones occurs due to the tendons and the ligaments connecting the bones, the CMC and the MCP have often been mathematically approximated, see [2, 3], and implemented, see [4, 5], in multibody models as universal joints, which means that the two axes of rotations are orthogonal and intersecting, as shown in Figure 1 (middle). Also, the flex-ext axis of the IP is assumed to be perpendicular to the sagittal plane of the thumb. However, a universal joint does not allow for the rotation of a single body along its longitudinal axis, which is observed in the thumb. Also in a study done by Valero-Cuevas, see [10], when compared with physical measurements, a thumb model with universal joints does not produce accurate forces at its tip in different postures. However, from the cadaveric measurements done by Hollister in [6] and [7], it was determined that the axes of the joints are neither orthogonal to each other or the bones nor intersecting with each other, as shown in Figure 1 (right). This was later confirmed by a number of studies through different methods, for example using optical measurements with surface markers, see [16, 17], or MRI, see [9, 18]. The CMC, MCP, IP flex-ext axes move with respect to the trapezium, the I MC, and the PP, respectively, while the CMC and MCP add-abd axes move with the I MC and the PP, respectively, see [6, 7, 8].

2.2. Thumb multibody model

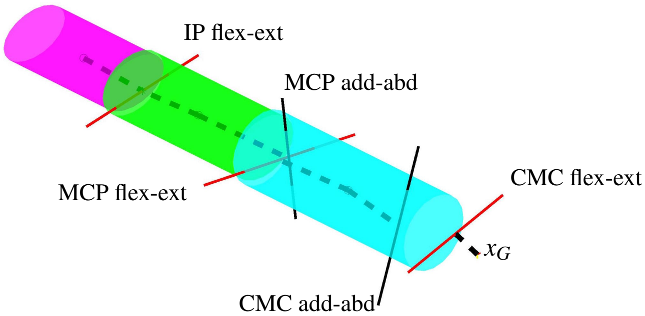

Figure 2: The thumb multibody model as described in Section 2.2. The I MC (cyan) is connected to ground x_G through the CMC (nino) joint. The PP (green) is connected to the I MC through the MCP (nino) joint. The DP (magenta) is connected to the PP through the IP (revolute) joint. The CMC flex-ext axis is proximal with respect to the CMC add-abd axis, while the MCP add-abd axis is proximal with respect to the MCP flex-ext axis.

Following the anatomy, the thumb multibody model, as shown in Figure 2 consists of three bodies, which are described in the director formulation, see [23]. To give a short overview, a rigid body in director formulation is described with its center of mass $\boldsymbol{\varphi} \in \mathbb{R}^3$ relative to an orthonormal basis $\{\mathbf{e}_I\}$ fixed in space and an orthonormal body frame called directors $\boldsymbol{d}_1, \boldsymbol{d}_2, \boldsymbol{d}_3 \in \mathbb{R}^3$ fixed at $\boldsymbol{\varphi}$. The time dependent configuration vector is given by $\boldsymbol{q}(t) = [\boldsymbol{\varphi}(t)\, \boldsymbol{d}_1(t)\, \boldsymbol{d}_2(t)\, \boldsymbol{d}_3(t)]^T \in \mathbb{R}^{12}$. A material point $\boldsymbol{\rho} \in \mathbb{R}^3$ in the body's configuration is described as $\boldsymbol{\rho}(t) = \rho_I \boldsymbol{d}_I(t)$. The orthonormality condition on the directors provides six internal constraints to the rigid body. The incremental kinematic update $\boldsymbol{u} \in \mathbb{R}^6, \boldsymbol{u}_{n+1} = \left(\boldsymbol{u}_{\boldsymbol{\varphi}_{n+1}},\ \boldsymbol{\theta}_{n+1}\right)$ for a rigid body to go from time-step n to $n+1$, is then given as

$$\boldsymbol{q}_{n+1} = \boldsymbol{F}_d\left(\boldsymbol{u}_{n+1},\ \boldsymbol{q}_n\right) = \left[\ \boldsymbol{\varphi}_n + \boldsymbol{u}_{\boldsymbol{\varphi}_{n+1}},\ \exp\left(\widehat{\boldsymbol{\theta}_{n+1}}\right)\cdot \boldsymbol{d}_{1n},\ \exp\left(\widehat{\boldsymbol{\theta}_{n+1}}\right)\cdot \boldsymbol{d}_{2n},\ \exp\left(\widehat{\boldsymbol{\theta}_{n+1}}\right)\cdot \boldsymbol{d}_{3n}\right]^T \tag{1}$$

where $\boldsymbol{u}_{\boldsymbol{\varphi}_{n+1}}$ is the increment in translation and $\boldsymbol{\theta}_{n+1}$ is the increment in rotation. The Rodrigues formula is used to obtain the exponential map, see [23].

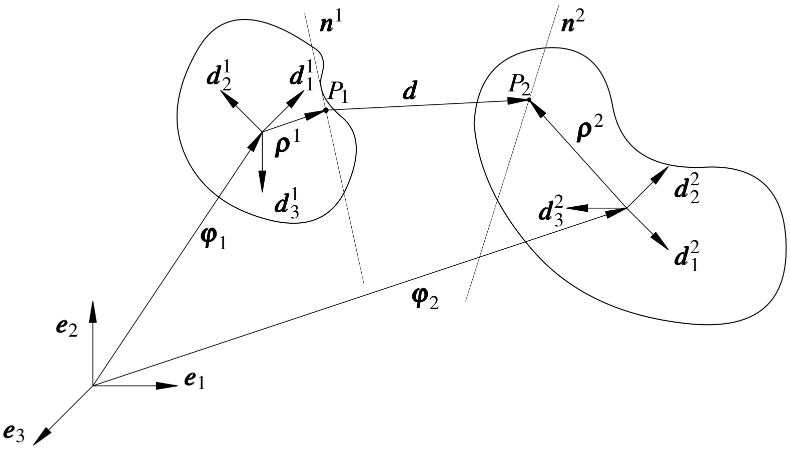

Figure 3: The kinematic pair with non-intersecting and non-orthogonal axes $\boldsymbol{n}^1$ and $\boldsymbol{n}^2$ between bodies with configuration vectors $\boldsymbol{q}^1$ and $\boldsymbol{q}^2$. The local vectors $\boldsymbol{\rho}^1$ and $\boldsymbol{\rho}^2$ define the locations of the points P_1 and P_2 for the axes $\boldsymbol{n}^1$ and $\boldsymbol{n}^2$, while the vector $\boldsymbol{d}$ connects these points. $\{\mathbf{e}_I\}$ is the spatially fixed orthonormal basis.

The IP joint is modeled as a revolute joint which has been described in [23]. The CMC and the MCP joints are modeled as joints with two axes which are non-intersecting and non-orthogonal (nino) to each other, as shown in Figure 3. It is a two degree of freedom joint with rotation axes $\boldsymbol{n}^1$ and $\boldsymbol{n}^2$, where $\boldsymbol{n}^1$ is fixed to the first body and $\boldsymbol{n}^2$ is fixed to the second body, $\boldsymbol{n}^1 = {n^1}_I \boldsymbol{d}_I^1$, $\boldsymbol{n}^2 = {n^2}_I \boldsymbol{d}_I^2$. A vector $\boldsymbol{d} = \boldsymbol{\varphi}^2 - \boldsymbol{\varphi}^1 + \boldsymbol{\rho}^2 - \boldsymbol{\rho}^1$ joins the points P_1 and P_2 which define the locations for axes $\boldsymbol{n}^1$ and $\boldsymbol{n}^2$, respectively. This kinematic pair gives rise to a constraint vector with four external constraints, as described for a universal joint in [11], between the rigid bodies with configuration vectors $\boldsymbol{q}^1$ and $\boldsymbol{q}^2$ as

$$\boldsymbol{g}(\boldsymbol{q}) = \begin{bmatrix} \|\boldsymbol{\varphi}^2 - \boldsymbol{\varphi}^1 + \boldsymbol{\rho}^2 - \boldsymbol{\rho}^1\|^2 - \|\boldsymbol{d}\|^2_{initial} \\ \boldsymbol{n}^1 \cdot \boldsymbol{d} - \left(\boldsymbol{n}^1 \cdot \boldsymbol{d}\right)_{initial} \\ \boldsymbol{n}^2 \cdot \boldsymbol{d} - \left(\boldsymbol{n}^2 \cdot \boldsymbol{d}\right)_{initial} \\ \boldsymbol{n}^1 \cdot \boldsymbol{n}^2 - \left(\boldsymbol{n}^1 \cdot \boldsymbol{n}^2\right)_{initial} \end{bmatrix} = \boldsymbol{0} \in \mathbb{R}^4 \tag{2}$$

wherein the first constraint keeps the distance between the points P_1 and P_2 constant. The second and third constraints keep the relative orientation of the non-intersecting and non-orthogonal axes $\boldsymbol{n}^1$ and $\boldsymbol{n}^2$, with the vector $\boldsymbol{d}$ constant. The last constraint keeps the angle between the two axes constant. The kinematic update for the nino joint, through an increment $\boldsymbol{u}_{n+1} = \left(\boldsymbol{u}_{\boldsymbol{\varphi}_{n+1}},\ \boldsymbol{\theta}_{n+1},\ \theta^1_{n+1},\ \theta^2_{n+1}\right) \in \mathbb{R}^8$, where θ^1_{n+1} and θ^2_{n+1} are the incremental rotation around axes $\boldsymbol{n}^1$ and $\boldsymbol{n}^2$, respectively, is given as

$$\boldsymbol{q}_{n+1} = \boldsymbol{F}_d\left(\boldsymbol{u}_{n+1},\ \boldsymbol{q}_n\right) = \begin{bmatrix} \boldsymbol{\varphi}_n + \boldsymbol{u}_{\boldsymbol{\varphi}_{n+1}} \\ \exp\left(\widehat{\boldsymbol{\theta}_{n+1}}\right) \cdot \boldsymbol{d}^1_{1n} \\ \exp\left(\widehat{\boldsymbol{\theta}_{n+1}}\right) \cdot \boldsymbol{d}^1_{2n} \\ \exp\left(\widehat{\boldsymbol{\theta}_{n+1}}\right) \cdot \boldsymbol{d}^1_{3n} \\ \boldsymbol{\varphi}_n + \boldsymbol{u}_{\boldsymbol{\varphi}_{n+1}} + \exp\left(\widehat{\boldsymbol{\theta}_{n+1}}\right) \cdot \left(\boldsymbol{\rho}^1_n + \exp\left(\widehat{\theta^1_{n+1}\boldsymbol{n}^1_n}\right) \cdot \boldsymbol{d}_n - \exp\left(\widehat{\theta^1_{n+1}\boldsymbol{n}^1_n}\right) \cdot \exp\left(\widehat{\theta^2_{n+1}\boldsymbol{n}^2_n}\right) \cdot \boldsymbol{\rho}^2_n\right) \\ \exp\left(\widehat{\boldsymbol{\theta}_{n+1}}\right) \cdot \exp\left(\widehat{\theta^1_{n+1}\boldsymbol{n}^1_n}\right) \cdot \exp\left(\widehat{\theta^2_{n+1}\boldsymbol{n}^2_n}\right) \cdot \boldsymbol{d}^2_{1n} \\ \exp\left(\widehat{\boldsymbol{\theta}_{n+1}}\right) \cdot \exp\left(\widehat{\theta^1_{n+1}\boldsymbol{n}^1_n}\right) \cdot \exp\left(\widehat{\theta^2_{n+1}\boldsymbol{n}^2_n}\right) \cdot \boldsymbol{d}^2_{2n} \\ \exp\left(\widehat{\boldsymbol{\theta}_{n+1}}\right) \cdot \exp\left(\widehat{\theta^1_{n+1}\boldsymbol{n}^1_n}\right) \cdot \exp\left(\widehat{\theta^2_{n+1}\boldsymbol{n}^2_n}\right) \cdot \boldsymbol{d}^2_{3n} \end{bmatrix} \tag{3}$$

The dimensions of the bones, i.e. the lengths and the radii of the bone in the radial and palmar directions and the locations and orientations of the axes of rotation of the joints have been obtained from a cadaver studies from Santos, see [12], and from Hollister, see [6, 7], respectively. The three joints have limitations on their motions, which have been documented by a number of researchers, using different methods, see [2, 20, 21]. The angle limit values in this paper have been taken from [13].

To describe in detail the complexity of the measurement adopting to multibody models, an example is provided. Hollister in 1992 provided measurements for locations and orientations of the CMC axes from seven cadaver thumbs. The add-abd axis of the CMC, as shown in Figure 4 (left), is located in the head of the I MC. In the study, its location in two directions is specified with ratios (or percentages) which helps in scaling the model, while the orientation is reported with angles with respect to the anatomical planes. These measurements are described with a mean $\pm$ standard deviation with a high anatomical variance, as shown in the table in Figure 4 (right), which gives little insight into the distribution of the values.

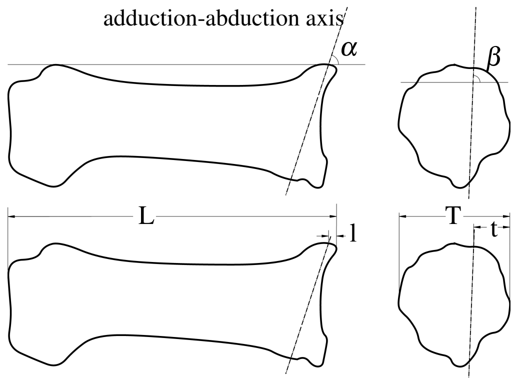

t/T	$59.5 \pm 14.3\%$
l/L	$12.5 \pm 6.2\%$
α	$83.6 \pm 14.2°$
β	$78.3 \pm 12.9°$

Figure 4: The CMC adduction-abduction axis, reproduced here from [6], is located in the head of the I MC (left). The orientation of the axis is defined with angles α and β. The location of the axis is defined with two length ratios t/T and l/L. The values are shown in the table (right), taken from [6].

To understand this variance, which depicts the natural variation in the human population, a Monte-Carlo study was performed by Santos, see [12]. The study concluded that the anatomical variation converges to four multi-modal distributions of distinct thumb models, shown in Figure 5 along with the base thumb model, named as types I, II, III and IV and described in Denavit-Hartenberg (D-H) notation, see [19]. These models have biomechanically distinct different kinematic features, namely in types I and IV, which comprise 65.2% of the population, the flex-ext axis of the MCP is distal to its add-abd axis, while it is opposite in the other 34.8%. The next level of differences involves the common normals, as described in the D-H notation, to the distal axis of the MCP and the flex-ext axis of the IP. Specifically, the common normal to the MCP distal axis points dorsally in type I and palmarly in type IV, while the common normal to the IP axis points proximally in type II and distally in type III. The base model, as named in Section 1, is created using the mean values of all the above mentioned cadaver measurements.

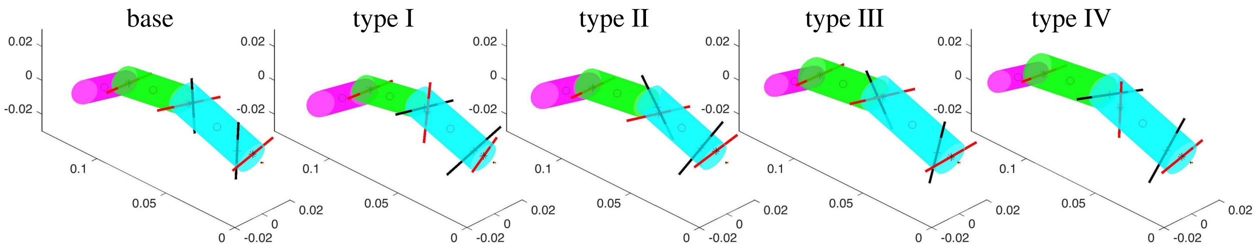

Figure 5: The different thumb models used to compare validation results. The base model is created with the mean values from cadaver measurements. The models named as types I, II, III and IV are taken from [12]. The models have differences in the axes locations and orientations. For example, the base, type II and type III models have the MCP add-abd axis proximal with respect to its flex-ext, when compared with type I and type IV models. The other differences are explained in Section 2.2.

2.3. Range of motion

The RoM of the thumb has been investigated in a number of studies, e.g. [2, 20]. However, they do not provide information such as location of the axes around which the angles are measured, or provide specification of the values of total flex-ext motion instead of only flexion or extension values (similar for add-abd angles), like in [14]. Furthermore, some use the assumption that the CMC and/or the MCP joints are modeled as universal joints and provide the Euler (cardan) angles ranges, as done in [2, 20]. Moreover, the studies which describe the axes do not provide the range of motion values. A comparative study of the RoM angles given by different researchers was done by [13] and [16], for the maximum RoM, which is the maximum extent to which the bones can be moved.

However, we also have limits on the range of motion with respect to grasping activity. Grasping cannot be performed with the fingers in their extreme positions, for example, holding a kettle or a basketball with a flat hand is not possible. To quantify the grasp RoM, a study was done [20] to measure the RoM for six grasps, namely tip pinch, palm pinch, lateral pinch, cylindrical grip, spherical grip and power grip. It is necessary to mention the caveat that postprocessing to describe the angles from these measurements was done using Euler angles and not around the actual axes of rotation. This RoM data was further post-processed, see [13], to determine the grasp RoM limits. The values for the maximum RoM and grasp RoM are tabulated in Table 1.

Table 1: Ranges of motion, taken from [13].

joint	maximum RoM		grasp RoM	
	flex-ext	add-abd	flex-ext	add-abd
CMC	-20°– 25°	-20°– 20°	-16°– 8°	-10°– 15°
MCP	-60°– 10°	-15°– 15°	-24°– 23°	-23°– 6°
IP	-60°– 20°	–	-49°– 0°	–

3. Validation techniques

For validation, there have been attempts to compare kinematics with a thumb modelled with universal joints, e.g. see [17], or to compare the Hausdorff distances in moving the first metacarpal from an initial posture to a particular posture, see [9]. Also, with the addition of muscles and tendons to the kinematic model, validation checks have been demonstrated with thumb kinetics, by comparing muscle moment arms, see [16], or the forces in the thumb tips for different postures, see [22]. Here, we use two techniques to compare the kinematic performance of the thumb, without resorting to marker-based physical measurements or introducing muscles in the model. These techniques on the one

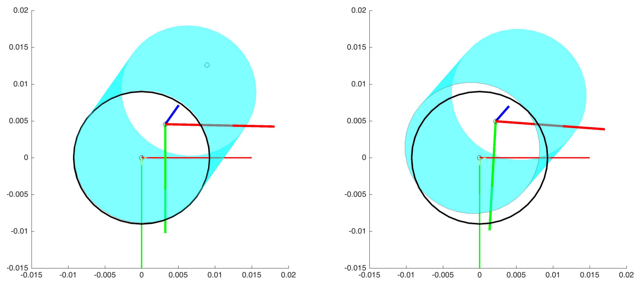

Figure 6: The motion of the I MC under combined rotations with the CMC joint modeled as a universal joint (left) and a nino joint (right). The thin red and green lines with the black circle as the cross section of the I MC show the initial configuration. The thick lines with corresponding colors show the cross-section of the I MC under combined flexion and adduction motions, which are parallel to the thin lines for the universal joint (left) and rotated around the blue joint for the nino joint (right) visualizing the resulting internal rotation.

hand quantify the reach of the end effector for grasping and, on the other hand, verify the rotation of the thumb metacarpal which is essential for thumb opposition.

3.1. RoM volume reduction for grasping

In the first technique, we quantify the point cloud workspace of the thumb tip. The point clouds are generated for all the five models for the maximum and the grasp RoMs. A quantitative indicator for the different point clouds of the thumb tip can simply be its encompassing volume. These volumes can be computed using α-shape, which is "a generalization of the convex hull of a finite set of points in the plane" (quoted from [24]). For a set S in $\mathbb{R}^3$, e.g. thumb tip end effector points, with a real constant $0 \leq \alpha \leq \infty$, an α-shape is the space generated by point pairs that can be touched by a sphere of radius α. Also, we have $\lim_{\alpha \to 0} S_\alpha = S$ and $\lim_{\alpha \to \infty} S_\alpha = \text{conv } S$, which is the convex hull for S. For detailed definition and explanation, see [24].

3.2. Thumb internal rotation

In the second technique, we compute the internal rotation of the I MC of the thumb models for different postures. A visual idea of the thumb rotation can be obtained while performing opposition from an extended position. Facing the palm, in the extended position the thumb DP pulp is seen, but with the thumb in opposed position, the pulp now touches the palm. Another example can be seen in the I MC behavior under combined rotation of flex-ext and add-abd. When compared to CMC joint modeled as a universal joint as shown in Figure 6 (left), the internal rotation of the cross-section of the I MC is clearly visible with the CMC joint modeled as a nino joint, as shown in Figure 6 (right). The complete internal rotation of the thumb is majorly contributed by the CMC joint, as compared to the MCP and the IP, see [17, 20]. Hence, a verification of the behavior of the thumb CMC under combined flex-ext and add-abd should give a reasonable idea about the thumb internal rotation performance.

4. Results

After describing the two validation schemes, the results for the two tests are reported.

4.1. RoM volume reduction for grasping

To generate a point cloud, the thumb model is kinematically moved through all its DoFs and a set is created with the thumb tip points in all positions. The ranges of angles, as given in Table 1, for every DoF are partitioned with 13 divisions to obtain a set of kinematic inputs to achieve a unique position. A point cloud with the thumb tip points is created for the base model and maximum RoM, as shown in Figure 7. It is observed that the α-shape volume does not change significantly with more divisions.

Using an α-shape radius of 0.5, the point cloud is enveloped with a smooth α-shape with no holes and the volume of the α-shape is computed. The point clouds are created for the base model and the four anatomically variable models from [12], which are converted from the D-H notation to the director formulation. This conversion is done to employ these models for calculating internal rotation of the I MC, which is readily possible as the directors of the I MC form the necessary rotation matrix. The volumes are computed for both the maximum and grasp ranges of motion. The α-shapes from point clouds for all the thumb models with the maximum and grasp RoM are shown in Figure 8. The

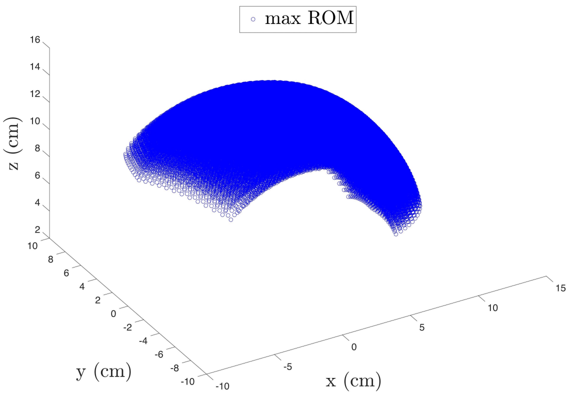

Figure 7: The point cloud for base model with maximum RoM.

volumes for all the point clouds are tabulated in Table 2. The volumes for the D-H models was computed and presented in [13], and is also given here in Table 2 for comparison.

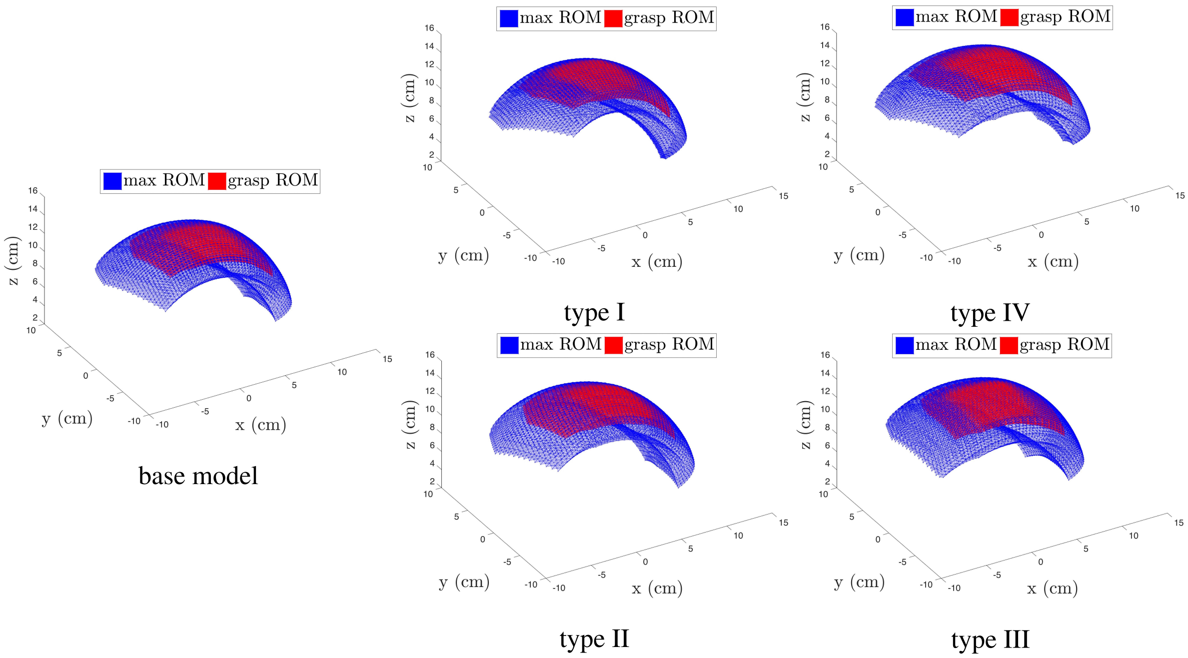

Figure 8: α-shapes for all models with maximum and grasp RoM.

From Figure 8, the overall shapes of the α-shapes look similar, which suggests different individuals with different thumbs can cover a similar work-space shape and can perform similar functions. However, on closer observations, differences between the edges and corners are apparent. Also the grasp volume α-shapes lie completely within the maximum volume α-shapes for the respective model, while having different shape than the grasp RoM α-shapes for the other models. The differences are much more evident in the volume reduction for the two RoMs, which we evaluate as the percentage reduction in volume for grasp RoM with respect to maximum RoM to compare the different models. It suggests individuals with model type III can cover more volume for grasping, however they are less effective in terms of the percentage of its grasping capacity, when compared to the model type I. A key observation from the values in Table 2 is that the volume and volume reduction for the base model lies within the range of anatomically variable models suggesting that a base model created with the mean values from cadaver measurements can be one realistic representation for a thumb model.

4.2. Thumb internal rotation

The internal rotation in the I MC is measured for different postures by Cooney, see [2], using T-shaped surface markers. The angles are measured with respect to a set initial position with the help of Euler angles, with the order of flex-ext,

Table 2: Volume results from our simulation and from [13].

	type I		type II		type III		type IV		base
	our	[13]	our	[13]	our	[13]	our	[13]	
volume maximum RoM (cm^3)	319.9	320	390.8	391	508.0	517	493.1	493	386.3
volume grasp RoM (cm^3)	100.1	103	104.2	106	129.6	123	123.2	122	99.3
% reduction	68.7	68	73.3	73	74.45	76	75.0	75	74.3

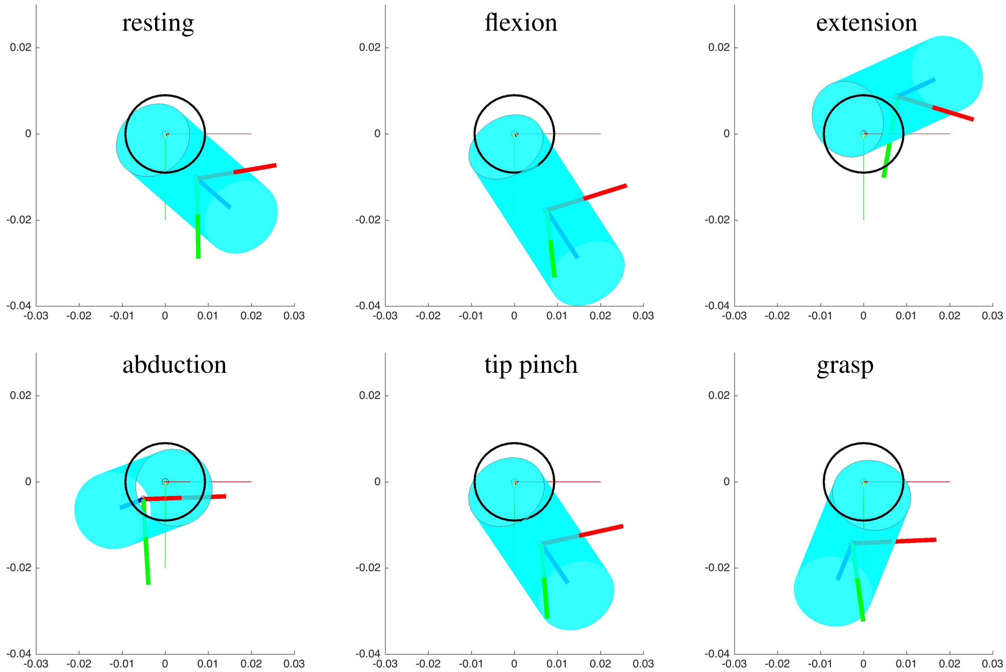

Figure 9: The movement of the I MC is shown for the different postures. Each posture results from a combination of pure flexion (downwards), pure extension (upwards), pure adduction (right) and pure abduction (left). The black circle shows the cross section of the I MC in the initial position.

add-abd followed by pro-sup and were expressed with a mean $\pm$ standard-deviation. As the inputs to the multibody models are given with respect to the rotation axes, the input angles are adjusted to arrive at the measured Euler angle input mean values for a particular posture. This adjustment was possible for all postures for all models, except for type I model for the extension posture. The different postures simulated are shown in Figure 9 and the values for all the different postures are presented in Table 3. Note that the terms flexion, extension, and abduction in Figure 9 and Table 3 are taken from Cooney, see [2], and do not imply pure motions around their axes, rather a combination.

For the measured values, all postures except extension indicate that the pronation of the I MC as the complete range of measured values is negative. As per Cooney, see [2], during extension it was observed that the thumb supinates from the resting position, which is supported by the measurements, as for extension posture there are a set of measured values in the range which are positive. The internal rotation values for the base model lies outside the range of the measured values, though it follows the pro-sup trend for all postures. This is also reflected in the simulation results for the anatomically variable values as well, with the additional observation that the pro-sup trend is not always followed by the types I, II and III. For example, for types I and II for resting posture, the I MC supinates instead of undergoing pronation, and for type III for abduction posture the I MC pronates instead of undergoing supination. However, type IV model follows the same trend as the measured and base model results. The difference of simulation results can be explained through the errors introduced by the use of surface markers made during the measurement process. It is observed that there can be angular differences of upto 4.9 degrees between the motion of the bone and the skin surfaces for the CMC joint, see [25]. This was also observed during total RoM measurement, see [17], with a difference of 7 degrees and 11 degrees for the flex-ext and add-abd RoMs respectively between the bone surface and skin surface markers. Also, for the grasp posture, Cooney [2] made the subjects wrap their thumb fingers around a cylinder of 3.5 centimeters in diameter. It has been suggested, see [20], that while grasping, the thumb bones may undergo passive rotations, to obtain a better grip of the object, while the simulation here can account for active motions only.

Table 3: Simulation results (all models) for internal rotation of I MC compared with measurements from [2].

	input angles		internal rotation (sup(+)–pro(-))					
				simulation				
posture	ext(+)–flx(-)	add(+)–abd(-)	measured	base	type I	type II	type III	type IV
resting	-20.5±10°	23.2±5°	-13.6±9°	-0.04°	3.99°	3.83°	-3.41°	-2.26°
flexion	-35.5±12°	21.3±6°	-19.5±7°	-5.13°	-8.73°	-0.66°	-4.15°	-6.86°
extension	12.6±7°	26±8°	-2.8±9°	10.2°	–	13.34°	-1.14°	7.95°
abduction	-6.2±10°	-15.6±12°	-19.5±12°	-3.52°	-9.13°	-4.55°	1.11°	-1.29°
tip pinch	-28±13°	18.2±10°	-18.7±10°	-3.87°	-5.39°	-0.41°	-3.41°	-5.4°
grasp	-24.6±16°	-9.8±8°	-19.8±8°	-7.14°	-15.6°	-7.08°	-0.69°	-5.63°

5. Conclusion

The thumb anatomy is very complex with a set of non-intersecting and non-orthogonal axes defining the joint systems which connect the three bones. This five DoF model, coupled with the high natural variance in the human population and the variability in the description and data reported by different researchers makes modeling a single ‘one-thumb-for-all’ very challenging. Hence, to develop a multibody model of the hand for grasping simulations, with a view to capture correct thumb motions, validation of the thumb kinematics is essential. The validation results from the point cloud volumes suggest that the thumb model created using the mean values from cadaver measurements can be useful with regards to defining the reach of the thumb. The volume and volume reduction results for this base model lies within the ranges of anatomically variable models. This is important as it indicates that a thumb model with such measurements and dimensions has as much grasping capacity as any thumb from the human population. With respect to the internal rotation of the I MC by imparting motion to the flex-ext and add-abd axes, the results follow the pro-sup trend with respect to the measured values, with a gross underestimation. This underestimation is also exhibited by the anatomically variable models. The internal rotation can be further verified by comparing with measurements from other studies, preferably measured with bone surface as opposed to skin surface markers. After a thorough verification of the CMC joint behavior, the thumb can be implemented to create a multibody model of the hand with the muscle-tendon network for the application of solving multi-point contact problems when formulating the grasp as an optimal control problem.

Acknowledgments

This work was supported by the Fraunhofer Internal Programs under Grant No. MAVO 828424.

References

[1] P. N. Soucacos, "Indications and selection for digitial amputation and replanatation", *The Journal of Hand Surgery: British & European Volume*, vol. 26, no. 6, pp. 572-581, 2001.

[2] W. P. Cooney, M. J. Lucca, E. Y. Chao and R. L. Linscheid, "The kinesiology of the thumb trapeziometacarpal joint", *The Journal of Bone and Joint Surgery*, vol. 63, no. 9, pp. 1371-1381, 1981.

[3] I. A. Kapandji, Biomechanics of the thumb. in: The Hand. vol. 1. Saunders, Philadelphia, 1981.

[4] J. Z. Wu, K. N. An, R. G. Cutlip, M. E. Andrew and R. G. Dong, "Modeling of the muscle/tendon excursions and moment arms in the thumb using the commercial software anybody", *Journal of Biomechanics*, vol. 42, no. 3, pp. 383-388, 2009.

[5] J. L. Sancho-Bru, M. C. Mora, B. E. León, A. Pérez-González, J. L. Iserte and A. Morales, "Grasp modelling with a biomechanical model of the hand", *Computer Methods in Biomechanics and Biomedical Engineering*, vol. 17, no. 4, pp. 297-310, 2014.

[6] A. Hollister, W. L. Buford, L. M. Myers, D. J. Giurintano and A. Novick, "The axes of rotation of the thumb carpometacarpal joint", *Journal of Orthopaedic Research*, vol. 10, no. 3, pp. 454-460, 1992.

[7] A. Hollister, D. J. Giurintano, W. L. Buford, L. M. Myers and A Novick, "The axes of rotation of the thumb interphalangeal and metacarpophalangeal joints", *Clinical Orthopaedics and Related Research* no. 320, pp. 188-193, 1995.

[8] D. J. Giurintano, A. M. Hollister, W. L. Buford, D. E. Thompson and L. M. Myers, "A virtual five-link model of the thumb", *Medical Engineering & Physics*, vol. 17, no. 4, pp. 297-303, 1995.

[9] P. Cerveri, E. De Momi, M. Marchente, G. Baud-Bovy, P. Scifo, R. M. L. Barros and G. Ferrigno, "Method for the estimation of a double hinge kinematic model for the trapeziometacarpal joint using MR imaging", *Computer Methods in Biomechanics and Biomedical Engineering*, vol. 13, no. 3, pp. 387-396, 2010.

[10] F. J. Valero-Cuevas, M. E. Johanson and J. D. Towles, "Towards a realistic biomechanical model of the thumb: the choice of kinematic description may be more critical than the solution method or the variability/uncertainty of musculoskeletal parameters", *Journal of Biomechanics*, vol. 36, no. 7, pp. 1019-1030, 2003.

[11] R. Maas and S. Leyendecker, "Biomechanical optimal control of human arm motion", *Journal of Multi-body Dynamics*, vol. 227, no. 4, pp. 375-389, 2013.

[12] V. J. Santos and F. J. Valero-Cuevas, "Reported anatomical variability naturally leads to multimodal distributions of Denavit-Hartenberg parameters for the human thumb", *IEEE Transactions on Biomedical Engineering*, vol. 53, no. 2, pp. 155-163, 2006.

[13] K. Dermitzakis, A. Ioannides, and H.-T. Lin, "Robotic thumb grasp-based range of motion optimisation", in *35th Annual International Conference of the IEEE Engineering in Medicine and Biology Society (EMBC)*, Osaka, 2013.

[14] J. J. Crisco, E. Halilaj, D. C. Moore, T. Patel, A.-P. C. Weiss and A. L .Ladd, "In Vivo Kinematics of the Trapeziometacarpal Joint During Thumb Extension-flexion and Abduction-adduction", *The Journal of Hand Surgery*, vol. 40, no. 2, pp. 289-296, 2015.

[15] L. Y. Chang and N. Pollard, "Method for determining kinematic parameters of the in vivo thumb carpometacarpal joint", *IEEE Transactions on Biomedical Engineering*, vol. 55, no. 7, pp. 1897-1906, 2008.

[16] L. Y. Chang and Y. Matsuoka, "A kinematic thumb model for the ACT hand", in *Proceedings 2006 IEEE International Conference on Robotics and Automation*, Orlando, Florida, 2006.

[17] P. Cerveri, E. De Momi, M. Marchente, N. Lopomo, G. Baud-Bovy, R. M. L. Barros and G. Ferrigno. "In Vivo Validation of a Realistic Kinematic Model for the Trapezio-Metacarpal Joint Using an Optoelectronic System", *Annals of Biomedical Engineering*, vol. 36, no. 7, pp. 1268–1280, 2008.

[18] C. Stillfried, U. Hillenbrand, M. Settles and P. van der Smagt, MRI-Based Skeletal Hand Movement Model in The Human Hand as an Inspiration for Robot Hand Development, Springer, 2014.

[19] R. S. Hartenberg, J. Denavit. Kinematic synthesis of linkages, McGraw-Hill, 1964.

[20] H.-T. Lin, L.-C. Kuo, H.-Y. Liu, W.-L. Wu and F.-C. Su, "The three-dimensional analysis of three thumb joints coordination in activities of daily living", *Clinical Biomechanics*, vol. 26, no. 4, pp. 371-376, 2011.

[21] Z.-M. Li and J. Tang, "Coordination of thumb joints during opposition", *Journal of Biomechanics*, vol. 40, no. 3, pp. 502-510, 2007.

[22] C. M. Goehler and W. M. Murray, "The sensitivity of endpoint forces produced by the extrinsic muscles of the thumb to posture", *Journal of Biomechanics*, vol. 43, no. 8, pp. 1553-1559, 2010.

[23] P. Betsch and S. Leyendecker, "The discrete null space method for the energy consistent integration of constrained mechanical systems. Part II: Multibody dynamics", *International Journal for Numerical Methods in Engineering*, vol. 67, pp. 499-552, 2006.

[24] H. Edelsbrunner, D. Kirkpatrick and R. Seidel, "On the shape of a set of points in the plane", *IEEE Transactions on Information Theory*, vol. 29, no. 4, pp. 551-559, 1983.

[25] L.-C. Kuo, W. P. Cooney III, M. Oyama, K. R. Kaufman, F.-C. Su and K.-N. An, "Feasibility of using surface markers for assessing motion of the thumb trapeziometacarpal joint", *Clinical Biomechanics*, vol. 18, no. 6, pp. 558-563, 2003.

[26] A. A. Samadani, D. Kulić and R. Gorbet "Multi-constrained inverse kinematics for the human hand", in *Engineering in Medicine and Biology Society (EMBC), 2012 Annual International Conference of the IEEE*, San Diego, California, 2012.